DESY–05–017
January, 2005

Forward jet production in deep inelastic ep scattering and low-x parton dynamics at HERA

ZEUS Collaboration

Abstract

Differential inclusive jet cross sections in neutral current deep inelastic ep scattering have been measured with the ZEUS detector using an integrated luminosity of 38.7 pb^{-1}. The jets have been identified using the k_T cluster algorithm in the longitudinally invariant inclusive mode in the laboratory frame; they have been selected with jet transverse energy, $E_T^{\rm jet}$, above 6 GeV and jet pseudorapidity, $\eta^{\rm jet}$, between -1 and 3. Measurements of cross sections as functions of $E_T^{\rm jet}$, $\eta^{\rm jet}$, Bjorken x and the photon virtuality, Q^2, are presented. Three phase-space regions have been selected in order to study parton dynamics from the most global to the most restrictive region of forward-going (close to the proton-beam direction) jets at low x, where the effects of BFKL evolution might be present. The measurements have been compared to the predictions of leading-logarithm parton-shower Monte Carlo models and fixed-order perturbative QCD calculations. In the forward region, $\mathcal{O}(\alpha_s^1)$ QCD calculations underestimate the data up to an order of magnitude at low x. An improved description of the data in this region is obtained by including $\mathcal{O}(\alpha_s^2)$ QCD corrections, which account for the lowest-order $\hat{t}$-channel gluon-exchange diagrams, highlighting the importance of such terms in the parton dynamics at low x.

The ZEUS Collaboration

S. Chekanov, M. Derrick, S. Magill, S. Miglioranzi[1], B. Musgrave, J. Repond, R. Yoshida
Argonne National Laboratory, Argonne, Illinois 60439-4815, USA [n]

M.C.K. Mattingly
Andrews University, Berrien Springs, Michigan 49104-0380, USA

N. Pavel, A.G. Yagües Molina
Institut für Physik der Humboldt-Universität zu Berlin, Berlin, Germany

P. Antonioli, G. Bari, M. Basile, L. Bellagamba, D. Boscherini, A. Bruni, G. Bruni, G. Cara Romeo, L. Cifarelli, F. Cindolo, A. Contin, M. Corradi, S. De Pasquale, P. Giusti, G. Iacobucci, A. Margotti, A. Montanari, R. Nania, F. Palmonari, A. Pesci, A. Polini, L. Rinaldi, G. Sartorelli, A. Zichichi
University and INFN Bologna, Bologna, Italy [e]

G. Aghuzumtsyan, D. Bartsch, I. Brock, S. Goers, H. Hartmann, E. Hilger, P. Irrgang, H.-P. Jakob, O. Kind, U. Meyer, E. Paul[2], J. Rautenberg, R. Renner, K.C. Voss[3], M. Wang, M. Wlasenko
Physikalisches Institut der Universität Bonn, Bonn, Germany [b]

D.S. Bailey[4], N.H. Brook, J.E. Cole, G.P. Heath, T. Namsoo, S. Robins
H.H. Wills Physics Laboratory, University of Bristol, Bristol, United Kingdom [m]

M. Capua, A. Mastroberardino, M. Schioppa, G. Susinno, E. Tassi
Calabria University, Physics Department and INFN, Cosenza, Italy [e]

J.Y. Kim, K.J. Ma[5]
Chonnam National University, Kwangju, South Korea [g]

M. Helbich, Y. Ning, Z. Ren, W.B. Schmidke, F. Sciulli
Nevis Laboratories, Columbia University, Irvington on Hudson, New York 10027 [o]

J. Chwastowski, A. Eskreys, J. Figiel, A. Galas, K. Olkiewicz, P. Stopa, D. Szuba, L. Zawiejski
Institute of Nuclear Physics, Cracow, Poland [i]

L. Adamczyk, T. Bołd, I. Grabowska-Bołd, D. Kisielewska, A.M. Kowal, J. Łukasik, M. Przybycień, L. Suszycki, J. Szuba[6]
Faculty of Physics and Applied Computer Science, AGH-University of Science and Technology, Cracow, Poland [p]

A. Kotański[7], W. Słomiński
Department of Physics, Jagellonian University, Cracow, Poland

V. Adler, U. Behrens, I. Bloch, K. Borras, G. Drews, J. Fourletova, A. Geiser, D. Gladkov, P. Göttlicher[8], O. Gutsche, T. Haas, W. Hain, C. Horn, B. Kahle, U. Kötz, H. Kowalski, G. Kramberger, D. Lelas[9], H. Lim, B. Löhr, R. Mankel, I.-A. Melzer-Pellmann, C.N. Nguyen, D. Notz, A.E. Nuncio-Quiroz, A. Raval, R. Santamarta, U. Schneekloth, U. Stösslein, G. Wolf, C. Youngman, W. Zeuner
Deutsches Elektronen-Synchrotron DESY, Hamburg, Germany

S. Schlenstedt
Deutsches Elektronen-Synchrotron DESY, Zeuthen, Germany

G. Barbagli, E. Gallo, C. Genta, P. G. Pelfer
University and INFN, Florence, Italy [e]

A. Bamberger, A. Benen, F. Karstens, D. Dobur, N.N. Vlasov[10]
Fakultät für Physik der Universität Freiburg i.Br., Freiburg i.Br., Germany [b]

P.J. Bussey, A.T. Doyle, J. Ferrando, J. Hamilton, S. Hanlon, D.H. Saxon, I.O. Skillicorn
Department of Physics and Astronomy, University of Glasgow, Glasgow, United Kingdom [m]

I. Gialas[11]
Department of Engineering in Management and Finance, Univ. of Aegean, Greece

T. Carli, T. Gosau, U. Holm, N. Krumnack[12], E. Lohrmann, M. Milite, H. Salehi, P. Schleper, T. Schörner-Sadenius, S. Stonjek[13], K. Wichmann, K. Wick, A. Ziegler, Ar. Ziegler
Hamburg University, Institute of Exp. Physics, Hamburg, Germany [b]

C. Collins-Tooth[14], C. Foudas, C. Fry, R. Gonçalo[15], K.R. Long, A.D. Tapper
Imperial College London, High Energy Nuclear Physics Group, London, United Kingdom [m]

M. Kataoka[16], K. Nagano, K. Tokushuku[17], S. Yamada, Y. Yamazaki
Institute of Particle and Nuclear Studies, KEK, Tsukuba, Japan [f]

A.N. Barakbaev, E.G. Boos, N.S. Pokrovskiy, B.O. Zhautykov
Institute of Physics and Technology of Ministry of Education and Science of Kazakhstan, Almaty, Kazakhstan

D. Son
Kyungpook National University, Center for High Energy Physics, Daegu, South Korea [g]

J. de Favereau, K. Piotrzkowski
Institut de Physique Nucléaire, Université Catholique de Louvain, Louvain-la-Neuve, Belgium [q]

F. Barreiro, C. Glasman[18], O. González, M. Jimenez, L. Labarga, J. del Peso, J. Terrón, M. Zambrana
Departamento de Física Teórica, Universidad Autónoma de Madrid, Madrid, Spain [l]

M. Barbi, F. Corriveau, C. Liu, S. Padhi, M. Plamondon, D.G. Stairs, R. Walsh, C. Zhou
Department of Physics, McGill University, Montréal, Québec, Canada H3A 2T8 [a]

T. Tsurugai
Meiji Gakuin University, Faculty of General Education, Yokohama, Japan [f]

A. Antonov, P. Danilov, B.A. Dolgoshein, V. Sosnovtsev, A. Stifutkin, S. Suchkov
Moscow Engineering Physics Institute, Moscow, Russia [j]

R.K. Dementiev, P.F. Ermolov, L.K. Gladilin, I.I. Katkov, L.A. Khein, I.A. Korzhavina, V.A. Kuzmin, B.B. Levchenko, O.Yu. Lukina, A.S. Proskuryakov, L.M. Shcheglova, D.S. Zotkin, S.A. Zotkin
Moscow State University, Institute of Nuclear Physics, Moscow, Russia [k]

I. Abt, C. Büttner, A. Caldwell, X. Liu, J. Sutiak
Max-Planck-Institut für Physik, München, Germany

N. Coppola, G. Grigorescu, S. Grijpink, A. Keramidas, E. Koffeman, P. Kooijman, E. Maddox, A. Pellegrino, S. Schagen, H. Tiecke, M. Vázquez, L. Wiggers, E. de Wolf
NIKHEF and University of Amsterdam, Amsterdam, Netherlands [h]

N. Brümmer, B. Bylsma, L.S. Durkin, T.Y. Ling
Physics Department, Ohio State University, Columbus, Ohio 43210 [n]

P.D. Allfrey, M.A. Bell, A.M. Cooper-Sarkar, A. Cottrell, R.C.E. Devenish, B. Foster, G. Grzelak, C. Gwenlan[19], T. Kohno, S. Patel, P.B. Straub, R. Walczak
Department of Physics, University of Oxford, Oxford United Kingdom [m]

P. Bellan, A. Bertolin, R. Brugnera, R. Carlin, R. Ciesielski, F. Dal Corso, S. Dusini, A. Garfagnini, S. Limentani, A. Longhin, L. Stanco, M. Turcato
Dipartimento di Fisica dell' Università and INFN, Padova, Italy [e]

E.A. Heaphy, F. Metlica, B.Y. Oh, J.J. Whitmore[20]
Department of Physics, Pennsylvania State University, University Park, Pennsylvania 16802 [o]

Y. Iga
Polytechnic University, Sagamihara, Japan [f]

G. D'Agostini, G. Marini, A. Nigro
Dipartimento di Fisica, Università 'La Sapienza' and INFN, Rome, Italy [e]

J.C. Hart
Rutherford Appleton Laboratory, Chilton, Didcot, Oxon, United Kingdom [m]

H. Abramowicz[21], A. Gabareen, S. Kananov, A. Kreisel, A. Levy
Raymond and Beverly Sackler Faculty of Exact Sciences, School of Physics, Tel-Aviv University, Tel-Aviv, Israel [d]

M. Kuze
Department of Physics, Tokyo Institute of Technology, Tokyo, Japan [f]

S. Kagawa, T. Tawara
Department of Physics, University of Tokyo, Tokyo, Japan [f]

R. Hamatsu, H. Kaji, S. Kitamura[22], K. Matsuzawa, O. Ota, Y.D. Ri
Tokyo Metropolitan University, Department of Physics, Tokyo, Japan [f]

M. Costa, M.I. Ferrero, V. Monaco, R. Sacchi, A. Solano
Università di Torino and INFN, Torino, Italy [e]

M. Arneodo, M. Ruspa
Università del Piemonte Orientale, Novara, and INFN, Torino, Italy [e]

S. Fourletov, T. Koop, J.F. Martin, A. Mirea
Department of Physics, University of Toronto, Toronto, Ontario, Canada M5S 1A7 [a]

J.M. Butterworth[23], R. Hall-Wilton, T.W. Jones, J.H. Loizides[24], M.R. Sutton[4], C. Targett-Adams, M. Wing
Physics and Astronomy Department, University College London, London, United Kingdom [m]

J. Ciborowski[25], P. Kulinski, P. Łużniak[26], J. Malka[26], R.J. Nowak, J.M. Pawlak, J. Sztuk[27], T. Tymieniecka, A. Tyszkiewicz[26], A. Ukleja, J. Ukleja[28], A.F. Żarnecki
Warsaw University, Institute of Experimental Physics, Warsaw, Poland

M. Adamus, P. Plucinski
Institute for Nuclear Studies, Warsaw, Poland

Y. Eisenberg, D. Hochman, U. Karshon, M.S. Lightwood
Department of Particle Physics, Weizmann Institute, Rehovot, Israel [c]

A. Everett, D. Kçira, S. Lammers, L. Li, D.D. Reeder, M. Rosin, P. Ryan, A.A. Savin, W.H. Smith
Department of Physics, University of Wisconsin, Madison, Wisconsin 53706, USA [n]

S. Dhawan
Department of Physics, Yale University, New Haven, Connecticut 06520-8121, USA [n]

S. Bhadra, C.D. Catterall, Y. Cui, G. Hartner, S. Menary, U. Noor, M. Soares, J. Standage, J. Whyte
Department of Physics, York University, Ontario, Canada M3J 1P3 [a]

[1] also affiliated with University College London, UK
[2] retired
[3] now at the University of Victoria, British Columbia, Canada
[4] PPARC Advanced fellow
[5] supported by a scholarship of the World Laboratory Björn Wiik Research Project
[6] partly supported by Polish Ministry of Scientific Research and Information Technology, grant no.2P03B 12625
[7] supported by the Polish State Committee for Scientific Research, grant no. 2 P03B 09322
[8] now at DESY group FEB, Hamburg, Germany
[9] now at LAL, Université de Paris-Sud, IN2P3-CNRS, Orsay, France
[10] partly supported by Moscow State University, Russia
[11] also affiliated with DESY
[12] now at Baylor University, USA
[13] now at University of Oxford, UK
[14] now at the Department of Physics and Astronomy, University of Glasgow, UK
[15] now at Royal Holloway University of London, UK
[16] also at Nara Women's University, Nara, Japan
[17] also at University of Tokyo, Japan
[18] Ramón y Cajal Fellow
[19] PPARC Postdoctoral Research Fellow
[20] on leave of absence at The National Science Foundation, Arlington, VA, USA
[21] also at Max Planck Institute, Munich, Germany, Alexander von Humboldt Research Award
[22] present address: Tokyo Metropolitan University of Health Sciences, Tokyo 116-8551, Japan
[23] also at University of Hamburg, Germany, Alexander von Humboldt Fellow
[24] partially funded by DESY
[25] also at Łódź University, Poland
[26] Łódź University, Poland
[27] Łódź University, Poland, supported by the KBN grant 2P03B12925
[28] supported by the KBN grant 2P03B12725

[a] supported by the Natural Sciences and Engineering Research Council of Canada (NSERC)

[b] supported by the German Federal Ministry for Education and Research (BMBF), under contract numbers HZ1GUA 2, HZ1GUB 0, HZ1PDA 5, HZ1VFA 5

[c] supported in part by the MINERVA Gesellschaft für Forschung GmbH, the Israel Science Foundation (grant no. 293/02-11.2), the U.S.-Israel Binational Science Foundation and the Benozyio Center for High Energy Physics

[d] supported by the German-Israeli Foundation and the Israel Science Foundation

[e] supported by the Italian National Institute for Nuclear Physics (INFN)

[f] supported by the Japanese Ministry of Education, Culture, Sports, Science and Technology (MEXT) and its grants for Scientific Research

[g] supported by the Korean Ministry of Education and Korea Science and Engineering Foundation

[h] supported by the Netherlands Foundation for Research on Matter (FOM)

[i] supported by the Polish State Committee for Scientific Research, grant no. 620/E-77/SPB/DESY/P-03/DZ 117/2003-2005 and grant no. 1P03B07427/2004-2006

[j] partially supported by the German Federal Ministry for Education and Research (BMBF)

[k] supported by RF Presidential grant N 1685.2003.2 for the leading scientific schools and by the Russian Ministry of Education and Science through its grant for Scientific Research on High Energy Physics

[l] supported by the Spanish Ministry of Education and Science through funds provided by CICYT

[m] supported by the Particle Physics and Astronomy Research Council, UK

[n] supported by the US Department of Energy

[o] supported by the US National Science Foundation

[p] supported by the Polish Ministry of Scientific Research and Information Technology, grant no. 112/E-356/SPUB/DESY/P-03/DZ 116/2003-2005 and 1 P03B 065 27

[q] supported by FNRS and its associated funds (IISN and FRIA) and by an Inter-University Attraction Poles Programme subsidised by the Belgian Federal Science Policy Office

1 Introduction

Deep inelastic lepton scattering (DIS) off protons provides information on the parton distribution functions (PDFs) of the proton. For example, inclusive measurements of the cross section for the reaction $e + p \to e + \mathrm{X}$ as a function of the virtuality of the exchanged boson, Q^2, and of the Bjorken-x scaling variable, x, have been used to determine $F_2^p(x, Q^2)$ which, in turn, is analysed in a theoretical context to extract the proton PDFs. Perturbative QCD in the next-to-leading-order (NLO) approximation has been widely used to perform such extraction and to test the extent to which it is able to describe the data. Perturbative QCD can predict only the evolution of the PDFs in Q^2; several approximations have been developed depending on the expected importance of the different terms in the perturbative expansion. In the standard approach (DGLAP [1]), the evolution equations sum up all leading double logarithms in $\ln Q^2 \cdot \ln 1/x$ along with single logarithms in $\ln Q^2$ and are expected to be valid for x not too small. At low x, a better approximation is expected to be provided by the BFKL formalism [2] in which the evolution equations sum up all leading double logarithms along with single logarithms in $\ln 1/x$.

The DGLAP evolution equations have been tested extensively at HERA [3–9], and were found to describe the data, in general, very well. In particular, the striking rise of the measured $F_2^p(x, Q^2)$ at HERA with decreasing x can be accomodated in the DGLAP approach. On the other hand, the inclusive character of F_2 together with the dependence of the DGLAP predictions on the choice of the input form of the non-perturbative PDFs at $Q^2 = Q_0^2$ may obscure the underlying dynamics at low x. In order to probe the parton dynamics at low x, measurements of the partonic final state that highlight the differences predicted by the BFKL and DGLAP formalisms were suggested [10].

In the DGLAP formalism, the parton cascade that results from the hard scattering of the virtual photon with a parton from the proton is ordered in parton virtuality. This ordering along the parton ladder implies an ordering in transverse energy of the partons, E_T, with the parton participating in the hard scatter having the highest transverse energy. In the BFKL formalism, there is no strict ordering in virtuality or transverse energy (see Fig. 1a). Since the partons emitted at the bottom of the ladder are closest in rapidity to the outgoing proton, they manifest themselves as forward[1] jets. BFKL evolution predicts that a larger fraction of small x events will contain high-E_T forward jets than is predicted by DGLAP [10, 11].

In previous studies of forward jets in DIS [12–14], the data were compared to Monte

[1] The ZEUS coordinate system is a right-handed Cartesian system, with the Z axis pointing in the proton beam direction, referred to as the "forward direction", and the X axis pointing towards the centre of HERA. The coordinate origin is at the nominal interaction point.

Carlo simulations which model higher-order parton emissions using the DGLAP approach. These models do not describe the data. However, it was possible to obtain a better description of the data by adding a second E_T-ordered parton cascade on the photon side which is evolved according to the DGLAP equations; this resolved-photon contribution [15] leads to parton-parton scattering which can give rise to the production of high-E_T jets anywhere along the (double) ladder between the photon and the proton. The calculations based on the Colour Dipole Model (CDM) [16], which include parton emissions not ordered in transverse energy, also described the data. In a more recent analysis [8], fixed-order QCD calculations were compared to the data. The predictions fail to describe the measurements in the most forward region at low E_T and Q^2.

In this paper, measurements of differential inclusive jet cross sections in deep inelastic scattering are presented in three different phase-space regions, from the most global to the most restrictive region, where the contribution of events exhibiting BFKL characteristics should be enhanced. A novel method is introduced (see Section 2) to increase the sensitivity to additional parton radiation in the forward region while extending the region in x towards lower values. The jets were reconstructed using the k_T cluster algorithm [17] in the longitudinally invariant mode [18], instead of the cone algorithm used in previous studies [12–14], which allows a reduction of the theoretical uncertainty associated with matching the experimental and theoretical jet algorithms. Inclusive jet cross sections were measured as functions of the jet transverse energy, $E_T^{\rm jet}$, pseudorapidity, $\eta^{\rm jet}$, and the event variables Q^2 and x. The effects of higher-order terms in the parton cascade were explored by comparing the data to fixed-order QCD predictions using current parametrisations of the proton PDFs based on DGLAP evolution. In addition, the predictions of a leading-logarithm parton-shower model based on DGLAP evolution and those of an implementation of the colour-dipole model were also compared to the data.

2 Theoretical expectations and phase-space definitions

For a given e^+p centre-of-mass energy, $\sqrt{s}$, the cross section for neutral current (NC) deep inelastic ep scattering, $e^+p \to e^+ + \mathrm{X}$, depends on two independent kinematic variables, which are chosen to be Q^2 and the Bjorken scaling variable, x, where $Q^2 = -q^2$ and $x = Q^2/(2P \cdot q)$; P (q) is the four-momentum of the incoming proton (exchanged virtual boson, V^*, with $V = \gamma$ or Z^0). Other variables used to define the kinematics of the events are $y = Q^2/(xs)$ and γ_h, defined by $\cos\gamma_h = ((1-y)xE_p - yE_e)/((1-y)xE_p + yE_e)$, where E_p (E_e) is the energy of the incoming proton (positron).

Jet production in NC DIS at $\mathcal{O}(\alpha_s^0)$ proceeds via $V^*q \to q$; this process is referred to as

being of quark-parton-model (QPM) type. The hadronic final state consists of a single jet emerging at polar angle γ_h and balancing the transverse momentum of the scattered e^+ plus the remnant of the proton. The NLO QCD corrections of $\mathcal{O}(\alpha_s^1)$ consist of one-loop corrections to the process $V^*q \to q$ and the tree-level processes of boson-gluon fusion (BGF, $V^*g \to q\bar{q}$) and QCD-Compton (QCDC, $V^*q \to qg$). In BGF and QCDC, when the two final-state partons are sufficiently separated from each other, the hadronic final state consists of two jets plus the remnant of the proton.

The predictions of fixed-order QCD calculations convoluted with PDFs extracted using the DGLAP equations have the following features for inclusive jet production: a dominant contribution ($\mathcal{O}(\alpha_s^0)$) from single-jet events with $\theta^{\rm jet} = \gamma_h$ and a $\mathcal{O}(\alpha_s^1)$-suppressed contribution from dijet events. Since at low values of x the variable γ_h points toward the rear direction, the production of forward (having positive values of $\eta^{\rm jet}$) jets is suppressed. In this region BFKL predicts a higher forward-jet cross section than DGLAP. This effect can be further enhanced by suppressing the evolution in Q^2 by requiring $(E_T^{\rm jet})^2 \sim Q^2$.

Experimental studies of QCD using jet production in NC DIS at HERA are often performed in the Breit frame [19]. The analysis presented here was instead performed in the laboratory frame for two reasons. First, such an analysis provides access to low values of x: the requirement of a jet in the Breit frame with a given $E_T^{\rm jet}$ would demand a larger fraction of the proton's momentum than that of a jet (with the same $E_T^{\rm jet}$) in the laboratory frame. It is noted that, in the Breit frame, the exchanged virtual boson collides head-on with the proton and, therefore, the transverse momentum of a jet must be balanced by other jet(s). Second, the application of the jet algorithm in the laboratory frame benefits from the increased resolution for identifying jets in the forward region of the detector. Jet cross sections in the laboratory frame are theoretically well defined and NLO QCD calculations for such observables are well behaved [20].

To investigate the NLO QCD predictions in detail, three phase-space regions of inclusive jet production have been studied. The first region, called "global", was designed to be as inclusive as possible to keep the theoretical uncertainties small. This region was defined by the conditions:

- $Q^2 > 25$ GeV^2;
- $y > 0.04$;
- $E'_e > 10$ GeV, where E'_e is the energy of the scattered positron;
- at least one jet with $E_T^{\rm jet} > 6$ GeV and $-1 < \eta^{\rm jet} < 3$.

This phase-space region is expected to be dominated by QPM-type events.

A second phase-space region, called "BFKL", was defined by the following additional conditions:

- $\cos\gamma_h < 0$;
- at least one jet with $0 < \eta^{\rm jet} < 3$ and $0.5 < \frac{(E_T^{\rm jet})^2}{Q^2} < 2$.

The combination of the requirements $\gamma_h > 90^\circ$ and $\theta^{\rm jet} < 90^\circ$ suppresses the contribution from QPM-type events. This phase-space region is expected to be dominated by multi-jet events. The enhancement of the contribution from multi-jet events is done without an explicit requirement on the number of jets and, thereby, keeping events at low values of x. The requirement on $(E_T^{\rm jet})^2/Q^2$ restricts the jet kinematics to the region where the BFKL effects are expected to be large.

A third phase-space region, called "forward BFKL", was designed to investigate events with a very forward-going jet and was defined by requiring, in addition to the aforementioned cuts, at least one jet with $2 < \eta^{\rm jet} < 3$.

3 Experimental set-up

The data sample used in this analysis was collected with the ZEUS detector at HERA and corresponds to an integrated luminosity of 38.7 ± 0.6 pb^{-1}. During 1996-1997, HERA operated with protons of energy $E_p = 820$ GeV and positrons of energy $E_e = 27.5$ GeV. A detailed description of the ZEUS detector can be found elsewhere [21, 22]. A brief outline of the components that are most relevant for this analysis is given here.

Charged particle tracks are reconstructed in the central tracking detector (CTD) [23], which operates in a magnetic field of 1.43 T provided by a thin superconducting solenoid. The CTD consists of 72 cylindrical drift-chamber layers, organised in nine superlayers covering the polar-angle region $15^\circ < \theta < 164^\circ$. The transverse-momentum resolution for full-length tracks can be parameterised as $\sigma(p_T)/p_T = 0.0058 p_T \oplus 0.0065 \oplus 0.0014/p_T$, with p_T in GeV. The tracking system was used to measure the interaction vertex with a typical resolution along (transverse to) the beam direction of 0.4 (0.1) cm and to cross-check the energy scale of the calorimeter.

The high-resolution uranium–scintillator calorimeter (CAL) [24] covers 99.7% of the total solid angle and consists of three parts: the forward (FCAL, $2.6^\circ < \theta < 36.7^\circ$), the barrel (BCAL, $36.7^\circ < \theta < 129.1^\circ$) and the rear (RCAL, $129.1^\circ < \theta < 176.2^\circ$) calorimeters. Each part is subdivided transversely into towers and longitudinally into one electromagnetic section (EMC) and either one (in RCAL) or two (in BCAL and FCAL) hadronic sections (HAC). The smallest subdivision of the calorimeter is called a cell. Under test-beam conditions, the CAL single-particle relative energy resolutions were $\sigma(E)/E = 0.18/\sqrt{E}$ for electrons and $\sigma(E)/E = 0.35/\sqrt{E}$ for hadrons, with E in GeV.

The luminosity was measured from the rate of the bremsstrahlung process $ep \to e\gamma p$. The resulting small-angle energetic photons were measured by the luminosity monitor [25], a lead-scintillator calorimeter placed in the HERA tunnel at $Z = -107$ m.

4 Data selection and jet identification

A three-level trigger was used to select events online [22]. The NC DIS events were selected offline using criteria similar to those reported previously [26]. The main steps are outlined below.

The scattered positron candidate was identified from the pattern of energy deposits in the CAL. The E'_e and polar angle (θ_e) of the positron candidate were also determined from the CAL measurements, after correction for energy loss in inactive material in front of the CAL. The following requirements were imposed on the data sample:

- the reconstructed $Q^2 > 25$ GeV^2;
- a positron candidate of energy $E'_e > 10$ GeV. This cut ensured a high and well understood positron-finding efficiency and suppressed background from photoproduction events, in which the scattered positron escapes undetected in the rear beampipe;
- the vertex position, determined from CTD tracks, in the range $|Z_{\rm vtx}| < 50$ cm along the beam axis. This cut removed background events from non-ep interactions;
- $38 < (E - P_Z) < 65$ GeV, where E is the total energy measured in the CAL, $E = \sum_i E_i$, and P_Z is the Z component of the vector $\boldsymbol{p} = \sum_i E_i \boldsymbol{r_i}$; in both cases the sum runs over all CAL cells, E_i is the energy of the CAL cell i and $\boldsymbol{r_i}$ is a unit vector along the line joining the reconstructed vertex to the geometric centre of the cell i. This cut removed events with large initial-state radiation and further reduced the background from photoproduction events;
- $y_e < 0.95$, where $y_e = 1 - E'_e(1 - \cos\theta_e)/(2E_e)$. This condition removed events in which fake positron candidates from photoproduction background were found in the FCAL;
- $y_{\rm JB} > 0.04$, where $y_{\rm JB} = \sum_i E_i(1 - \cos\theta_i)/(2E_e)$ calculated according to the Jacquet-Blondel method [27], where the sum runs over all CAL cells except those assigned to the scattered positron. The $y_{\rm JB}$ variable is an estimator of y which gives a good resolution at low y;
- $p_T^{\rm CAL}/\sqrt{E_T^{\rm CAL}} < 3\ \sqrt{\rm GeV}$, where $p_T^{\rm CAL}$ is the total transverse momentum as measured with the CAL and $E_T^{\rm CAL}$ is the total transverse energy in the CAL. This cut removed cosmic rays and beam-related background;

- $|X| > 14$ cm or $|Y| > 14$ cm, where X and Y are the impact positions of the positron on the CAL, to avoid the low-acceptance region adjacent to the rear beampipe;
- the energy not associated with the positron candidate within a cone of radius 0.7 units in the pseudorapidity-azimuth ($\eta - \phi$) plane around the positron direction was required to be less than 10% of the positron energy. This condition removed photoproduction and DIS events in which a part of a jet was incorrectly identified as the scattered positron.

The kinematic variables Q^2 and x were reconstructed using a combination of the electron and double-angle (DA) methods [28], depending on which method gave a better resolution of the observed scattered-positron energy. The angle γ_h was reconstructed with the CAL using:

$$\cos\gamma_h = \frac{(\sum_i p_{X,i})^2 + (\sum_i p_{Y,i})^2 - (\sum_i (E - p_Z)_i)^2}{(\sum_i p_{X,i})^2 + (\sum_i p_{Y,i})^2 + (\sum_i (E - p_Z)_i)^2},$$

where the sum runs over all CAL cells, excluding those associated with the scattered positron.

The k_T cluster algorithm was used in the longitudinally invariant inclusive mode to reconstruct jets in the hadronic final state from the energy deposits in the CAL cells. The jet algorithm was applied after excluding those cells associated with the scattered-positron candidate. The jet search was performed in the $\eta - \phi$ space in the laboratory frame. The jet variables were defined according to the Snowmass convention [29]. Jet transverse energies were corrected for all energy-loss effects, principally in inactive material, typically about one radiation length, in front of the CAL. After these corrections to the jet transverse energy, events with at least one jet satisfying $E_T^{\rm jet} > 6$ GeV and $-1 < \eta^{\rm jet} < 3$ were included in the global data sample. The BFKL and forward-BFKL subsamples were selected using the additional requirements listed in Section 2.

5 Monte Carlo simulation

Samples of events were generated to determine the response of the detector to jets of hadrons and to determine the correction factors necessary to obtain the hadron-level jet cross sections. The generated events were passed through the GEANT 3.13-based [30] ZEUS detector- and trigger-simulation programs [22]. They were reconstructed and analysed by the same program chain as the data.

Neutral current DIS events were generated using the LEPTO 6.5.1 program [31] interfaced to HERACLES 4.6.1 [32] via DJANGOH 1.1 [33]. The HERACLES program includes photon and Z exchanges and first-order electroweak radiative corrections. The QCD cascade was modelled with the CDM as implemented in the ARIADNE 4.08 program [34]; ARIADNE

simulates the BGF process in addition. The CDM treats gluons emitted from quark-antiquark (diquark) pairs as radiation from a colour dipole between two partons. This results in partons that are not ordered in their transverse momenta. Samples of events were also generated using the model of LEPTO based on first-order QCD matrix elements plus parton showers (MEPS). For the generation of the samples with MEPS, the option for soft-colour interactions was switched off [35]. In both cases, fragmentation into hadrons was performed using the Lund string model [36] as implemented in JETSET 7.4 [37]. The CTEQ4M [38] proton PDFs were used for all simulations.

The jet identification was performed using the simulated energy measured in the CAL cells in the same way as for the data. The same jet algorithm was also applied to the final-state particles and to the partons available after the parton shower; the jets found in this way are referred to as hadronic and partonic jets, respectively.

Electroweak-radiative and hadronisation effects are not at present included in the fixed-order QCD programs described in Section 7. Therefore, samples of Monte Carlo (MC) events were generated with and without electroweak-radiative effects so that the data could be corrected. The samples without electroweak-radiative effects were used to correct the QCD calculations for hadronisation effects. Since the measurements refer to jets of hadrons, whereas the QCD calculations refer to partons, the predictions were corrected to the hadron level using these MC samples. A multiplicative correction factor, C_{had}, was defined as the ratio of cross sections for jets of hadrons over that for jets of partons, and was computed with the MC programs. The factor applied to the predictions was the average of the correction factors obtained with ARIADNE and LEPTO. The uncertainty on the hadronisation correction was taken to be the absolute difference in the correction factors obtained with ARIADNE and LEPTO.

6 Acceptance corrections and systematic uncertainties

The ARIADNE MC samples of events were used to compute the acceptance corrections. These correction factors took into account the efficiency of the trigger, the selection criteria, and the purity and efficiency of the jet identification, and were generally between 0.8 and 1.2. The inclusive cross sections for jets of hadrons were determined by applying bin-by-bin corrections to the measured distributions. For this approach to be valid, the distributions in the data must be well described by the MC simulations at the detector level. This condition was in general satisfied by both ARIADNE and LEPTO. The LEPTO MC samples were used to compute the systematic uncertainties coming from the parton-shower simulation.

A study of the main sources contributing to the systematic uncertainties of the measurements was performed [39]. These sources were:

- the parton-shower simulation. The effect of the treatment of the parton shower was estimated using LEPTO to evaluate the acceptance-correction factors. The difference in the corrected cross sections between using ARIADNE and LEPTO was taken to be the value of systematic uncertainty;
- the choice of reconstruction method for the kinematic variables Q^2 and x. The difference in the corrected cross sections between using the electron and double-angle methods was taken to be the value of systematic uncertainty;
- the biases introduced by the selection cuts. The uncertainty due to the selection requirements was computed by varying the values of the cuts in data and MC. The largest effects were due to the cuts on jet transverse energy and hadronic angle.

These systematic uncertainties were added in quadrature. The absolute energy scale of the jets in data events was varied by its uncertainty of 3% [40]. This uncertainty is highly correlated between measurements in different bins and is therefore treated separately. The largest contribution to the overall systematic uncertainty was due to the uncertainty in the jet energy scale, which averaged about 5%, but could reach values as high as 20%. The second-largest contribution was due to the choice of parton-shower simulation, which had effects on the corrected cross section generally below 5%; in the most restrictive phase space, however, the E_T^{jet}, x and Q^2 bins with the fewest events had large systematic differences. The uncertainty in the luminosity determination of 1.6% was not included.

7 QCD calculations

The measurements were compared with QCD predictions evaluated using the program DISENT [41]. The calculations were performed in the $\overline{\text{MS}}$ renormalisation and factorisation schemes using a generalised version of the subtraction method [41]. The number of flavors was set to five; the renormalisation (μ_R) and factorisation (μ_F) scales were both set to $\mu_R = \mu_F = Q$; α_s was calculated at two loops using $\Lambda^{(5)}_{\overline{\text{MS}}} = 226$ MeV, which corresponds to $\alpha_s(M_Z) = 0.1180$. The CTEQ6 [42] parameterisations of the proton PDFs were used. The results obtained with DISENT were cross-checked using the program DISASTER++ [43]; the differences were found to be less than 1% in most cases, and never exceeded 3%.

DISENT allows calculations that sum up to two orders of the perturbation series. In the global phase-space region, the sample is dominated by single-jet events. Therefore, the DISENT predictions in this region were calculated using the diagrams with $\mathcal{O}(\alpha_s^0)$ and

$\mathcal{O}(\alpha_s^1)$. In the BFKL and forward-BFKL phase-space regions, the samples consist of multijet events, and so the DISENT calculations were computed using terms with $\mathcal{O}(\alpha_s^1)$ and $\mathcal{O}(\alpha_s^2)$. Perturbative QCD calculations at $\mathcal{O}(\alpha_s^2)$ can give rise to forward jet production at low x through diagrams such as that shown in Fig. 1b, but no E_T-ordering is explicitely imposed among the three final-state partons.

The following sources of theoretical uncertainties were considered:

- the choice of renormalisation scale. The uncertainty in the calculations arising from the absence of higher-order terms was estimated by varying μ_R by a factor of two up and down. The effect on the calculations is between 5 and 50%, depending on the phase-space region;
- the uncertainties in the proton PDFs. The effect of these uncertainties in the calculations was estimated by repeating the calculations using 40 additional sets from CTEQ6. The resulting uncertainty was always below 5%;
- the choice of factorisation scale. The uncertainty in the calculations was estimated by varying μ_F by a factor of two up and down. The effect on the calculations was usually less than 5%, except in the global phase-space region where it contributed a 20% uncertainty at low x.

8 Results

The measurements of cross sections differential in X, where X is η^{jet}, E_T^{jet}, Q^2 or x, are presented in the three phase-space regions. The measured cross sections were corrected to hadron level by the formula:

$$\left(\frac{d\sigma}{dX}\right)_{\text{had}} = \frac{N_{\text{Data}}}{\mathcal{L}\cdot\Delta X}\cdot\frac{N_{\text{MC}}^{\text{had}}}{N_{\text{MC}}^{\text{det}}}\cdot\frac{N_{\text{MC}}^{\text{noQED}}}{N_{\text{MC}}^{\text{QED}}}$$

where ΔX is the bin size, N_{Data} are the numbers of data events, $\mathcal{L}$ is the integrated luminosity, $N_{\text{MC}}^{\text{had}}$ ($N_{\text{MC}}^{\text{det}}$) is the hadron- (detector-) level MC distribution, $N_{\text{MC}}^{\text{QED}}$ ($N_{\text{MC}}^{\text{noQED}}$) is the hadron-level MC distribution generated with (without) QED radiation.

The cross sections as functions of η^{jet} and E_T^{jet} are measurements of every jet in the event, whereas the cross sections as functions of Q^2 and x are event cross sections for the events in the inclusive jet samples.

8.1 The global phase-space region

The measurements in the global phase-space region are presented in Fig. 2 and Tables 1 to 4. The cross section as a function of η^{jet} is suppressed in the forward region (high η^{jet})

due to the lower cut on y. The measurements span x values between 0.00074 and 0.24.

The MC predictions and fixed-order QCD calculations are compared to the data in Fig. 2. The prediction of ARIADNE describes all data distributions well, whereas the predictions from LEPTO are slightly worse, especially at the lowest x values. The fixed-order QCD calculations describe the data at high $E_T^{\rm jet}$, Q^2 and x values. However, at low values of these variables, the calculations underestimate the data, and the $\eta^{\rm jet}$ distribution is not described, particularly at high values of $\eta^{\rm jet}$. This excess of the data with respect to the calculations can be due to the absence of higher orders, since these calculations are only $\mathcal{O}(\alpha_s)$. The small uncertainty coming from the variation of μ_R is not expected to be a reliable estimate of the contributions from higher orders: contributions from gluon exchange in the $\hat{t}$ channel (as shown in Fig. 1b), which become dominant at low x [44], appear only at higher orders, but their effects cannot be inferred from scale variations of the (lower) terms considered in the calculation.

8.2 The BFKL phase-space region

The measurements in the BFKL phase-space region are presented in Fig. 3 and Tables 5 to 8. The shape of the cross section as a function of $\eta^{\rm jet}$ is steeply falling in the forward region due to the restriction on γ_h. The predictions of ARIADNE describe all data distributions well. The predictions of LEPTO fail to describe the data, especially in the $\eta^{\rm jet}$ distribution and low-x region.

Fixed-order QCD calculations, which are $\mathcal{O}(\alpha_s^2)$ in this phase-space region, describe the data well for Q^2, $E_T^{\rm jet}$ and x, but underestimate the data at high values of $\eta^{\rm jet}$. This disagreement is concentrated in a region where the cross section is small, and so it is not reflected in the other distributions. The uncertainty of the calculations due to the absence of higher orders is larger than before, and is a more realistic estimation than in the global phase-space region: in the present case the calculation is $\mathcal{O}(\alpha_s^2)$, which contains the first contribution from $\hat{t}$-channel gluon-exchange diagrams (see Fig. 1b).

These features were investigated by comparing the LO ($\mathcal{O}(\alpha_s^1)$) and NLO ($\mathcal{O}(\alpha_s^2)$) calculations: a) the scale variation of the NLO calculation is reduced with respect to that of the LO calculation (not shown) for the cross sections, except for $d\sigma/d\eta^{\rm jet}$ in the region $\eta^{\rm jet} > 1$ and for $d\sigma/dx$ at low x, where it is larger; b) in these regions the NLO corrections are largest and the ratio NLO/LO reaches values as large as five for $\eta^{\rm jet} \sim 3$. The large increase of the cross section from LO to NLO at low x and large $\eta^{\rm jet}$ is associated with the contribution from $\hat{t}$-channel gluon-exchange diagrams [45]. The sizeable scale variation at NLO arises from the fact that such contributions come from tree-level diagrams with three final-state partons and, as a result, the calculation accounts in an effective way only

for the lowest-order contribution [45]. Thus, the cross-section calculations at low x and large $\eta^{\rm jet}$ are expected to be subjected to large corrections from higher-order terms.

8.3 The forward BFKL phase-space region

The measurements in the forward BFKL phase-space region are presented in Fig. 4 and Tables 9 to 11. Events exhibiting BFKL effects are expected to be dominant in this phase-space region. The predictions of ARIADNE describe the data well, whereas the predictions of LEPTO fail in all distributions. Fixed-order QCD calculations are consistently lower than the data for $E_T^{\rm jet}$ and Q^2. The calculations describe the measurement as a function of x at high values, but underestimate the data in the low-x region by nearly a factor of two. The features observed in the comparison of LO and NLO calculations in Section 8.2 are more dramatic in the present case: a) the scale variations of the NLO calculations are larger than those of LO calculations everywhere except at high x; b) the NLO corrections are large everywhere except at high x and the ratio NLO/LO reaches values as large as ten at low x. The increase of the cross-section calculations from LO to NLO, which brings the predictions closer to the data, is associated with the contribution from $\hat{t}$-channel gluon-exchange diagrams, which represent the lowest-order term of the expansion that leads to the BFKL resummation. The increased scale variation at NLO, which is larger by nearly a factor of two than that in the BFKL phase-space region, highlights the need for improved calculations.

9 Summary

Measurements of differential cross sections in $E_T^{\rm jet}$, $\eta^{\rm jet}$, Q^2 and x for inclusive jet production in neutral current deep inelastic scattering have been presented using 38.7 pb^{-1} of ZEUS data. The low-x region has been probed for events with $Q^2 > 25$ GeV^2 and at least one jet with $E_T^{\rm jet} > 6$ GeV. Three phase-space regions have been studied: one inclusive region (global phase space), one with an additional requirement on the hadronic angle of the event ($\cos\gamma_h < 0$) and a more limited window of jet pseudorapidity ($0 < \eta^{\rm jet} < 3$), as well as the requirement $0.5 < (E_T^{\rm jet})^2/Q^2 < 2.0$ (BFKL phase space), and finally the more restricted region with $2 < \eta^{\rm jet} < 3$ (forward BFKL phase space). The restrictions imposed in the BFKL phase-space regions enhance the multijet contributions without restricting the transverse energy of the parton(s) close to the hard scatter.

A large excess of the data over the fixed-order ($\mathcal{O}(\alpha_s)$) QCD calculation is observed in the global phase-space region at high $\eta^{\rm jet}$ and low x. This excess cannot be accomodated within the experimental and the estimated theoretical uncertainties. However, the size of

the higher-order terms might be underestimated since the scale variations cannot reflect the contributions from $\hat{t}$-channel gluon-exchange diagrams, which are expected to become dominant at low x.

In the BFKL phase-space region, the fixed-order ($\mathcal{O}(\alpha_s^2)$) QCD calculation gives, in general, a good description of the data except for $\eta^{\rm jet} > 2$, where an excess of the data over the prediction is observed. In this phase-space region, the NLO QCD corrections significantly reduce the scale variation of the predicted cross sections with respect to a LO calculation, except for $d\sigma/d\eta^{\rm jet}$ in the region $\eta^{\rm jet} > 1$ and for $d\sigma/dx$ at low x. In these regions, the NLO corrections, which account for the lowest-order contribution from $\hat{t}$-channel gluon-exchange diagrams, are largest and bring the calculations close to the data. However, the strong dependence of the calculations with the renormalisation scale is indicative of the importance of higher-order terms in these regions.

In the forward BFKL region, the fixed-order ($\mathcal{O}(\alpha_s^2)$) QCD calculation describes the shape of the measured differential cross sections $d\sigma/dE_T^{\rm jet}$ and $d\sigma/dQ^2$, but fails to describe that of $d\sigma/dx$. The restriction to the region $2 < \eta^{\rm jet} < 3$ enhances the contribution from $\hat{t}$-channel gluon-exchange diagrams, which increases the NLO prediction by up to a factor of ten at low x with respect to a LO calculation and brings it closer to the data. The variation of the calculations with the renormalisation scale is large, emphasizing the need for higher-order calculations. The improved description of the data in this region achieved by accounting for the lowest-order contribution from $\hat{t}$-channel gluon-exchange diagrams, highlights the importance of such terms in the parton dynamics at low x.

Acknowledgments

We thank the DESY Directorate for their strong support and encouragement. We are grateful for the support of the DESY computing and network services. The diligent efforts of the HERA machine group are gratefully acknowledged. The design, construction and installation of the ZEUS detector have been made possible due to the ingenuity and efforts of many people from DESY and other institutes who are not listed as authors.

References

[1] V.N. Gribov and L.N. Lipatov, Sov. J. Nucl. Phys. 15 (1972) 438;
L.N. Lipatov, Sov. J. Nucl. Phys. 20 (1975) 94;
Yu.L. Dokshitzer, Sov. Phys. JETP 46 (1977) 641;
G. Altarelli and G. Parisi, Nucl. Phys. B 126 (1977) 298.

[2] E.A. Kuraev, L.N. Lipatov and V.S. Fadin, Sov. Phys. JETP 45 (1977) 199;
Ya.Ya. Balitskiĭ and L.N. Lipatov, Sov. J. Nucl. Phys. 28 (1978) 822.

[3] ZEUS Coll., S. Chekanov et al., Phys. Rev. D 70 (2004) 052001.

[4] ZEUS Coll., S. Chekanov et al., Phys. Lett. B 547 (2002) 164.

[5] ZEUS Coll., S. Chekanov et al., Phys. Rev. D 67 (2003) 012007.

[6] ZEUS Coll., J. Breitweg et al., Phys. Lett. B 507 (2001) 70.

[7] H1 Coll., C. Adloff et al., Eur. Phys. J. C 30 (2003) 1.

[8] H1 Coll., C. Adloff et al., Phys. Lett. B 542 (2002) 193.

[9] H1 Coll., C. Adloff et al., Phys. Lett. B 515 (2001) 17.

[10] A.H. Mueller, Nucl. Phys. Proc. Suppl. C 18 (1991) 125;
A.H. Mueller, J. Phys. G 17 (1991) 1443.

[11] J. Bartels, A. De Roeck and M. Loewe, Z. Phys. C 54 (1992) 645;
J. Kwiecinski, A.D. Martin and P.J. Sutton, Phys. Lett. B 287 (1992) 254;
W.K. Tang, Phys. Lett. B 278 (1992) 363.

[12] ZEUS Coll., J. Breitweg et al., Eur. Phys. J. C 6 (1999) 239.

[13] ZEUS Coll., J. Breitweg et al., Phys. Lett. B 474 (2000) 223.

[14] H1 Coll., C. Adloff et al., Nucl. Phys. B 538 (1999) 3.

[15] H. Jung, Comp. Phys. Comm. 86 (1995) 147.

[16] Y. Azimov et al., Phys. Lett. B 165 (1985) 147;
G. Gustafson, Phys. Lett. B 175 (1986) 453;
G. Gustafson and U. Pettersson, Nucl. Phys. B 306 (1988) 746;
B. Andersson et al., Z. Phys. C 43 (1989) 625.

[17] S.Catani et al., Nucl. Phys. B406 (1993) 187.

[18] S.D. Ellis and D.E. Soper, Phys. Rev. D 48 (1993) 3160.

[19] R.P. Feynman, *Photon-Hadron Interactions*. Benjamin, New York, (1972).

[20] B. Poetter and M.H. Seymour, J. Phys. G 25 (1999) 1473.

[21] ZEUS Coll., M. Derrick et al., Phys. Lett. B 293 (1992) 465.

[22] ZEUS Coll., U. Holm (ed.), *The ZEUS Detector*. Status Report (unpublished), DESY (1993), available on `http://www-zeus.desy.de/bluebook/bluebook.html`.

[23] N. Harnew et al., Nucl. Inst. Meth. A 279 (1989) 290;
B. Foster et al., Nucl. Phys. Proc. Suppl. B 32 (1993) 181;
B. Foster et al., Nucl. Inst. Meth. A 338 (1994) 254.

[24] M. Derrick et al., Nucl. Inst. Meth. A 309 (1991) 77;
A. Andresen et al., Nucl. Inst. Meth. A 309 (1991) 101;
A. Caldwell et al., Nucl. Inst. Meth. A 321 (1992) 356;
A. Bernstein et al., Nucl. Inst. Meth. A 336 (1993) 23.

[25] J. Andruszków et al., Preprint DESY-92-066, DESY, 1992;
ZEUS Coll., M. Derrick et al., Z. Phys. C 63 (1994) 391;
J. Andruszków et al., Acta Phys. Pol. B 32 (2001) 2025.

[26] ZEUS Coll., S. Chekanov et al., Preprint hep-ex/0208037, 2002.

[27] F. Jacquet and A. Blondel, *Proc. of the Study for an ep Facility for Europe*, U. Amaldi (ed.), p. 391. Hamburg, Germany (1979). Also in preprint DESY 79/48.

[28] S. Bentvelsen, J. Engelen and P. Kooijman, *Proc. Workshop on Physics at HERA*, W. Buchmüller and G. Ingelman (eds.), Vol. 1, p. 23. Hamburg, Germany, DESY (1992).

[29] J.E. Huth et al., *Research Directions for the Decade. Proceedings of Summer Study on High Energy Physics, 1990*, E.L. Berger (ed.), p. 134. World Scientific (1992). Also in preprint FERMILAB-CONF-90-249-E.

[30] R. Brun et al., GEANT3, Technical Report CERN-DD/EE/84-1, CERN, 1987.

[31] G. Ingelman, A. Edin and J. Rathsman, Comp. Phys. Comm. 101 (1997) 108.

[32] A. Kwiatkowski, H. Spiesberger and H.-J. Möhring, Comp. Phys. Comm. 69 (1992) 155.

[33] K. Charchula, G.A. Schuler and H. Spiesberger, Comp. Phys. Comm. 81 (1994) 381;
H. Spiesberger, HERACLES *and* DJANGOH*: Event Generation for ep Interactions at HERA Including Radiative Processes*, 1998, available on `http://www.desy.de/~hspiesb/djangoh.html`.

[34] L. Lönnblad, Comp. Phys. Comm. 71 (1992) 15;
L. Lönnblad, Z. Phys. C 65 (1995) 285.

[35] ZEUS Coll., J. Breitweg et al., Eur. Phys. J. C 11 (1999) 251.

[36] B. Andersson et al., Phys. Rep. 97 (1983) 31.

[37] T. Sjöstrand, Comp. Phys. Comm. 82 (1994) 74.

[38] H.L. Lai et al., Phys. Rev. D 55 (1997) 1280.

[39] S. Lammers. Ph.D. Thesis, University of Wisconsin-Madison (2004) (unpublished).

[40] ZEUS Coll., S. Chekanov et al., Eur. Phys. J. C 23 (2002) 13.

[41] S. Catani and M.H. Seymour, Nucl. Phys. B 485, 291 (1997). Erratum in Nucl. Phys. **B 510**, 503 (1998).

[42] J. Pumplin et al., JHEP 0207 (2002) 012.

[43] D. Graudenz, Preprint hep-ph/9708362, 1997;
D. Graudenz, Preprint hep-ph/9710244, 1997.

[44] V. Del Duca, Preprint hep-ph/9707348, 1997.

[45] E. Mirkes and D. Zeppenfeld, Phys. Rev. Lett. 78 (1997) 428.

$\eta^{\rm jet}$ bin	$d\sigma/d\eta^{\rm jet}$ (pb)	Δ_{stat}	Δ_{syst}	$\Delta_{{\rm jet}-ES}$	QED correction	PAR to HAD correction
-1 – -0.5	2722	± 13	$^{+25}_{-46}$	$^{+162}_{-160}$	0.989	0.812 ± 0.004
-0.5 – 0	3788	± 13	$^{+36}_{-108}$	$^{+157}_{-161}$	0.972	0.842 ± 0.001
0 – 0.5	4362	± 14	$^{+71}_{-82}$	$^{+175}_{-178}$	0.956	0.856 ± 0.005
0.5 – 1	4791	± 15	$^{+38}_{-97}$	$^{+163}_{-175}$	0.951	0.880 ± 0.004
1 – 1.5	4217	± 16	$^{+24}_{-34}$	$^{+106}_{-109}$	0.947	1.025 ± 0.007
1.5 – 2	2538	± 11	$^{+18}_{-22}$	$^{+71}_{-71}$	0.953	1.12 ± 0.03
2 – 2.5	1323	± 8	$^{+25}_{-132}$	$^{+46}_{-45}$	0.959	1.02 ± 0.05
2.5 – 3	685	± 5	$^{+36}_{-74}$	$^{+39}_{-37}$	0.960	0.97 ± 0.05

Table 1: *Inclusive jet cross-section $d\sigma/d\eta^{\rm jet}$ for jets of hadrons in the global phase space. The statistical, systematic and jet-energy-scale uncertainties are shown separately. The multiplicative correction applied to correct for QED radiative effects and for hadronisation effects are shown in the last two columns.*

$E_T^{\rm jet}$ bin (GeV)	$d\sigma/dE_T^{\rm jet}$ (pb/GeV)	Δ_{stat}	Δ_{syst}	$\Delta_{{\rm jet}-ES}$	QED correction	PAR to HAD correction
6 – 8	2685	± 6	$^{+20}_{-72}$	$^{+26}_{-33}$	0.965	0.910 ± 0.006
8 – 10	1408	± 4	$^{+8}_{-36}$	$^{+53}_{-57}$	0.954	0.9163 ± 0.0005
10 – 14	599.9	± 1.9	$^{+4.5}_{-9.3}$	$^{+37.6}_{-36.3}$	0.957	0.917 ± 0.003
14 – 21	165.55	± 0.75	$^{+1.94}_{-2.40}$	$^{+12.51}_{-11.75}$	0.961	0.93 ± 0.02
21 – 29	40.59	± 0.35	$^{+0.83}_{-0.84}$	$^{+3.58}_{-3.82}$	0.956	0.94 ± 0.02
29 – 47	7.90	± 0.10	$^{+0.18}_{-0.21}$	$^{+0.82}_{-0.76}$	0.953	0.96 ± 0.01
47 – 71	0.873	± 0.030	$^{+0.052}_{-0.043}$	$^{+0.120}_{-0.095}$	0.966	0.965 ± 0.007
71 – 127	0.0433	± 0.0044	$^{+0.0080}_{-0.0047}$	$^{+0.0068}_{-0.0100}$	0.996	0.980 ± 0.001

Table 2: *Inclusive jet cross-section $d\sigma/dE_T^{\rm jet}$ for jets of hadrons in the global phase space. The statistical, systematic and jet-energy-scale uncertainties are shown separately. The multiplicative correction applied to correct for QED radiative effects and for hadronisation effects are shown in the last two columns.*

Q^2 bin (GeV^2)	$d\sigma/dQ^2$ ($\mathrm{pb/GeV}^2$)	Δ_{stat}	Δ_{syst}	$\Delta_{\mathrm{jet}-ES}$	QED correction	PAR to HAD correction
25 – 50	127.11	± 0.35	$^{+2.06}_{-8.64}$	$^{+8.46}_{-8.55}$	0.970	0.85 ± 0.01
50 – 100	73.26	± 0.20	$^{+0.66}_{-1.46}$	$^{+2.32}_{-2.47}$	0.961	0.937 ± 0.008
100 – 250	17.965	± 0.055	$^{+0.140}_{-0.174}$	$^{+0.139}_{-0.157}$	0.952	1.001 ± 0.001
250 – 630	2.550	± 0.013	$^{+0.019}_{-0.036}$	$^{+0.003}_{-0.004}$	0.947	1.0046 ± 0.0003
630 – 1600	0.3128	± 0.0028	$^{+0.0039}_{-0.0049}$	$^{+0.0002}_{-0.0003}$	0.934	1.003 ± 0.001
1600 – 4000	0.03072	± 0.00057	$^{+0.00091}_{-0.00060}$	$^{+0}_{-0}$	0.930	1.0004 ± 0.0009
4000 – 10^5	0.0001764	± 0.0000069	$^{+0.0000124}_{-0.0000092}$	$^{+0}_{-0}$	0.975	0.998 ± 0.002

Table 3: *Cross-section $d\sigma/dQ^2$ for events in the global phase space. The statistical, systematic and jet-energy-scale uncertainties are shown separately. The multiplicative correction applied to correct for QED radiative effects and for hadronisation effects are shown in the last two columns.*

x bin	$d\sigma/dx$ (nb)	Δ_{stat}	Δ_{syst}	$\Delta_{\mathrm{jet}-ES}$	QED correction	PAR to HAD correction
.0001 – .001	507.7	± 3.7	$^{+21.4}_{-48.8}$	$^{+28.8}_{-28.5}$	1.029	0.94 ± 0.03
.001 – .0025	1255.6	± 4.6	$^{+19.7}_{-114.3}$	$^{+73.8}_{-74.5}$	0.985	0.914 ± 0.002
.0025 – .0063	883.5	± 2.4	$^{+35.6}_{-22.4}$	$^{+40.3}_{-41.2}$	0.965	0.903 ± 0.004
.0063 – .0158	330.35	± 0.93	$^{+2.00}_{-2.61}$	$^{+6.11}_{-7.01}$	0.945	0.928 ± 0.002
.0158 – .04	60.22	± 0.26	$^{+0.42}_{-3.42}$	$^{+0.18}_{-0.19}$	0.942	0.9899 ± 0.0005
.04 – .1	7.607	± 0.056	$^{+0.064}_{-0.408}$	$^{+0.004}_{-0.002}$	0.922	0.9989 ± 0.0007
.1 – 1	0.1622	± 0.0023	$^{+0.0048}_{-0.0032}$	$^{+0.0001}_{-0.0001}$	0.914	0.99960 ± 0.00001

Table 4: *Cross-section $d\sigma/dx$ for events in the global phase space. The statistical, systematic and jet-energy-scale uncertainties are shown separately. The multiplicative correction applied to correct for QED radiative effects and for hadronisation effects are shown in the last two columns.*

$\eta^{\rm jet}$ bin	$d\sigma/d\eta^{\rm jet}$ (pb)	Δ_{stat}	Δ_{syst}	$\Delta_{{\rm jet}-ES}$	QED correction	PAR to HAD correction
0 – 0.5	2228	± 11	$^{+41}_{-50}$	$^{+74}_{-81}$	0.951	1.10 ± 0.02
0.5 – 1	869	± 7	$^{+22}_{-31}$	$^{+24}_{-24}$	0.977	1.10 ± 0.06
1 – 1.5	464	± 5	$^{+13}_{-40}$	$^{+21}_{-19}$	0.981	1.01 ± 0.04
1.5 – 2	339	± 4	$^{+10}_{-27}$	$^{+15}_{-18}$	0.973	0.98 ± 0.06
2 – 2.5	276	± 4	$^{+9}_{-30}$	$^{+14}_{-16}$	1.004	0.93 ± 0.06
2.5 – 3	186	± 3	$^{+11}_{-15}$	$^{+13}_{-14}$	0.993	0.93 ± 0.06

Table 5: *Inclusive jet cross-section $d\sigma/d\eta^{\rm jet}$ for jets of hadrons in the BFKL phase space. The statistical, systematic and jet-energy-scale uncertainties are shown separately. The multiplicative correction applied to correct for QED radiative effects and for hadronisation effects are shown in the last two columns.*

$E_T^{\rm jet}$ bin (GeV)	$d\sigma/dE_T^{\rm jet}$ (pb/GeV)	Δ_{stat}	Δ_{syst}	$\Delta_{{\rm jet}-ES}$	QED correction	PAR to HAD correction
6 – 8	619.0	± 2.9	$^{+10.3}_{-20.6}$	$^{+17.3}_{-17.2}$	0.967	1.06 ± 0.05
8 – 10	249.3	± 1.8	$^{+4.0}_{-6.9}$	$^{+10.8}_{-11.3}$	0.964	1.06 ± 0.03
10 – 14	77.76	± 0.73	$^{+2.64}_{-2.81}$	$^{+4.01}_{-4.61}$	0.964	1.08 ± 0.03
14 – 21	15.32	± 0.25	$^{+0.36}_{-0.95}$	$^{+1.00}_{-1.11}$	0.976	1.04 ± 0.04
21 – 29	2.325	± 0.089	$^{+0.170}_{-0.147}$	$^{+0.254}_{-0.292}$	0.951	1.052 ± 0.009
29 – 47	0.245	± 0.019	$^{+0.030}_{-0.033}$	$^{+0.031}_{-0.040}$	0.957	0.951 ± 0.004

Table 6: *Inclusive jet cross-section $d\sigma/dE_T^{\rm jet}$ for jets of hadrons in the BFKL phase space. The statistical, systematic and jet-energy-scale uncertainties are shown separately. The multiplicative correction applied to correct for QED radiative effects and for hadronisation effects are shown in the last two columns.*

Q^2 bin (GeV^2)	$d\sigma/dQ^2$ ($\mathrm{pb/GeV}^2$)	Δ_{stat}	Δ_{syst}	$\Delta_{\mathrm{jet}-ES}$	QED correction	PAR to HAD correction
25 – 50	35.62	± 0.20	$^{+0.98}_{-1.84}$	$^{+1.60}_{-1.58}$	0.967	1.01 ± 0.03
50 – 100	14.858	± 0.090	$^{+0.357}_{-0.528}$	$^{+0.431}_{-0.463}$	0.968	1.12 ± 0.04
100 – 250	2.121	± 0.020	$^{+0.074}_{-0.106}$	$^{+0.068}_{-0.070}$	0.954	1.15 ± 0.03
250 – 630	0.1868	± 0.0038	$^{+0.0077}_{-0.0118}$	$^{+0.0058}_{-0.0112}$	0.985	1.16 ± 0.02
630 – 1600	0.01262	± 0.00062	$^{+0.00082}_{-0.00155}$	$^{+0.00080}_{-0.00102}$	0.957	1.144 ± 0.003

Table 7: *Cross-section $d\sigma/dQ^2$ for events in the BFKL phase space. The statistical, systematic and jet-energy-scale uncertainties are shown separately. The multiplicative correction applied to correct for QED radiative effects and for hadronisation effects are shown in the last two columns.*

x bin	$d\sigma/dx$ (nb)	Δ_{stat}	Δ_{syst}	$\Delta_{\mathrm{jet}-ES}$	QED correction	PAR to HAD correction
.0001 – .001	145.6	± 1.9	$^{+6.2}_{-22.1}$	$^{+7.9}_{-8.5}$	1.023	0.90 ± 0.05
.001 – .0025	393.6	± 2.6	$^{+13.2}_{-25.0}$	$^{+15.8}_{-14.8}$	0.992	1.01 ± 0.05
.0025 – .0063	286.4	± 1.5	$^{+10.9}_{-14.0}$	$^{+9.6}_{-9.8}$	0.951	1.11 ± 0.02
.0063 – .0158	21.69	± 0.24	$^{+0.98}_{-1.46}$	$^{+0.55}_{-0.88}$	0.942	1.2282 ± 0.0001
.0158 – .04	0.591	± 0.025	$^{+0.041}_{-0.070}$	$^{+0.035}_{-0.054}$	0.944	1.18 ± 0.01

Table 8: *Cross-section $d\sigma/dx$ for events in the BFKL phase space. The statistical, systematic and jet-energy-scale uncertainties are shown separately. The multiplicative correction applied to correct for QED radiative effects and for hadronisation effects are shown in the last two columns.*

$E_T^{\rm jet}$ bin (GeV)	$d\sigma/dE_T^{\rm jet}$ (pb/GeV)	Δ_{stat}	Δ_{syst}	$\Delta_{{\rm jet}-ES}$	QED correction	PAR to HAD correction
6 – 8	75.5	± 1.0	$^{+3.4}_{-5.3}$	$^{+4.0}_{-4.3}$	0.997	0.91 ± 0.06
8 – 10	24.08	± 0.57	$^{+0.81}_{-1.94}$	$^{+1.58}_{-1.79}$	0.991	0.95 ± 0.06
10 – 14	6.08	± 0.20	$^{+0.29}_{-0.73}$	$^{+0.49}_{-0.58}$	0.999	0.99 ± 0.03
14 – 21	0.871	± 0.055	$^{+0.067}_{-0.083}$	$^{+0.062}_{-0.052}$	0.998	1.03 ± 0.07
21 – 29	0.081	± 0.016	$^{+0.032}_{-0.026}$	$^{+0.018}_{-0.012}$	0.922	1.01 ± 0.03

Table 9: *Inclusive jet cross-section $d\sigma/dE_T^{\rm jet}$ for jets of hadrons in the forward-BFKL phase space. The statistical, systematic and jet-energy-scale uncertainties are shown separately. The multiplicative correction applied to correct for QED radiative effects and for hadronisation effects are shown in the last two columns.*

Q^2 bin (GeV^2)	$d\sigma/dQ^2$ ($\mathrm{pb/GeV}^2$)	Δ_{stat}	Δ_{syst}	$\Delta_{\mathrm{jet}-ES}$	QED correction	PAR to HAD correction
25 – 50	4.650	± 0.075	$^{+0.190}_{-0.420}$	$^{+0.273}_{-0.320}$	0.992	0.93 ± 0.06
50 – 100	1.587	± 0.029	$^{+0.098}_{-0.092}$	$^{+0.106}_{-0.094}$	0.999	0.93 ± 0.06
100 – 250	0.1735	± 0.0053	$^{+0.0070}_{-0.0202}$	$^{+0.0094}_{-0.0108}$	0.984	0.96 ± 0.02
250 – 630	0.01093	± 0.00080	$^{+0.00103}_{-0.00180}$	$^{+0.00047}_{-0.00083}$	1.010	1.03 ± 0.01
630 – 1600	0.000414	± 0.000093	$^{+0.000170}_{-0.000126}$	$^{+0}_{-0.000041}$	0.944	1.04 ± 0.02

Table 10: *Cross-section $d\sigma/dQ^2$ for events in the forward-BFKL phase space. The statistical, systematic and jet-energy-scale uncertainties are shown separately. The multiplicative correction applied to correct for QED radiative effects and for hadronisation effects are shown in the last two columns.*

x bin	$d\sigma/dx$ (nb)	Δ_{stat}	Δ_{syst}	$\Delta_{\mathrm{jet}-ES}$	QED correction	PAR to HAD correction
.0001 – .001	36.4	± 1.1	$^{+3.0}_{-6.7}$	$^{+2.4}_{-2.2}$	1.066	0.88 ± 0.06
.001 – .0025	68.0	± 1.1	$^{+2.5}_{-6.2}$	$^{+4.1}_{-4.7}$	1.024	0.91 ± 0.07
.0025 – .0063	22.12	± 0.41	$^{+1.67}_{-1.70}$	$^{+1.46}_{-1.34}$	0.962	0.96 ± 0.04
.0063 – .0158	0.872	± 0.039	$^{+0.077}_{-0.066}$	$^{+0.026}_{-0.059}$	0.957	1.00 ± 0.03
.0158 – .04	0.01113	± 0.0021	$^{+0.0095}_{-0.0029}$	$^{+0}_{-0.0012}$	0.945	0.9 ± 0.1

Table 11: *Cross-section $d\sigma/dx$ for events in the forward-BFKL phase space. The statistical, systematic and jet-energy-scale uncertainties are shown separately. The multiplicative correction applied to correct for QED radiative effects and for hadronisation effects are shown in the last two columns.*

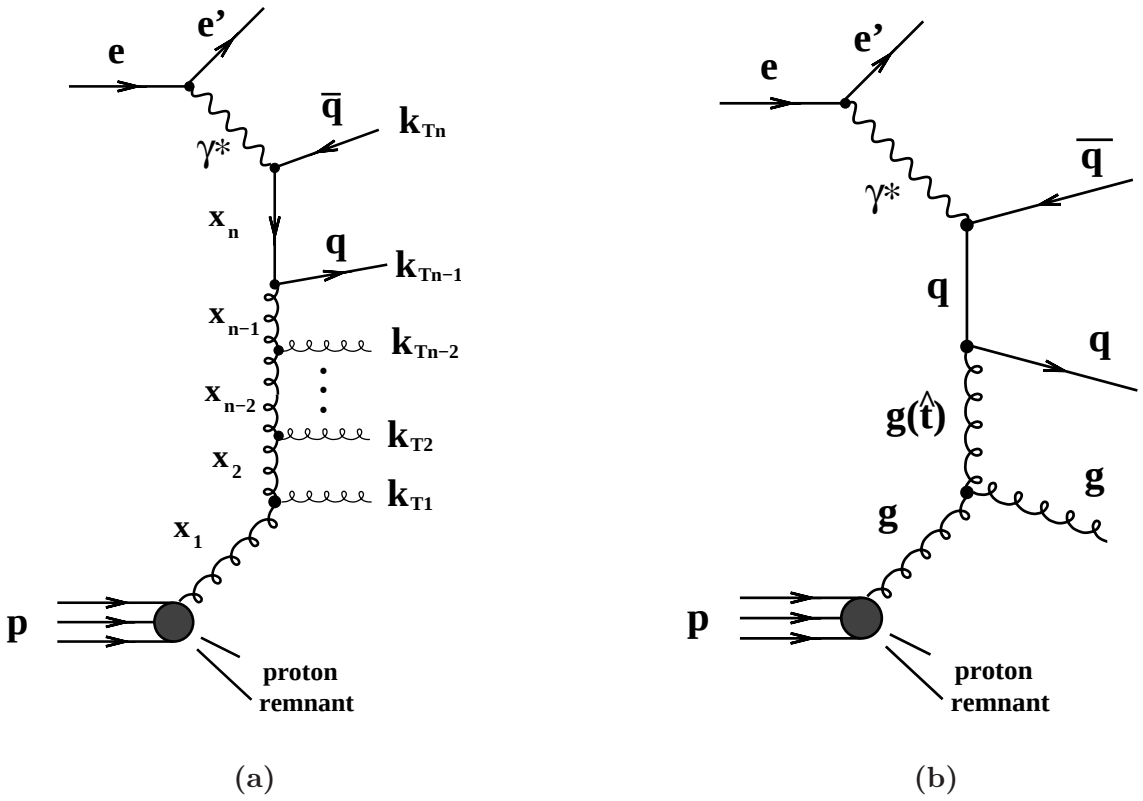

Figure 1: *(a) Gluon-ladder Feynman diagram. In DGLAP evolution, the final-state partons are ordered in transverse energy, $k^2_{T,n} > k^2_{T,n-1} > k^2_{T,1}$. In BFKL, the partons are emitted without any ordering in k_T along the ladder. (b) Example of Feynman diagram with $\hat{t}$-channel gluon exchange at $\mathcal{O}(\alpha_s^2)$.*

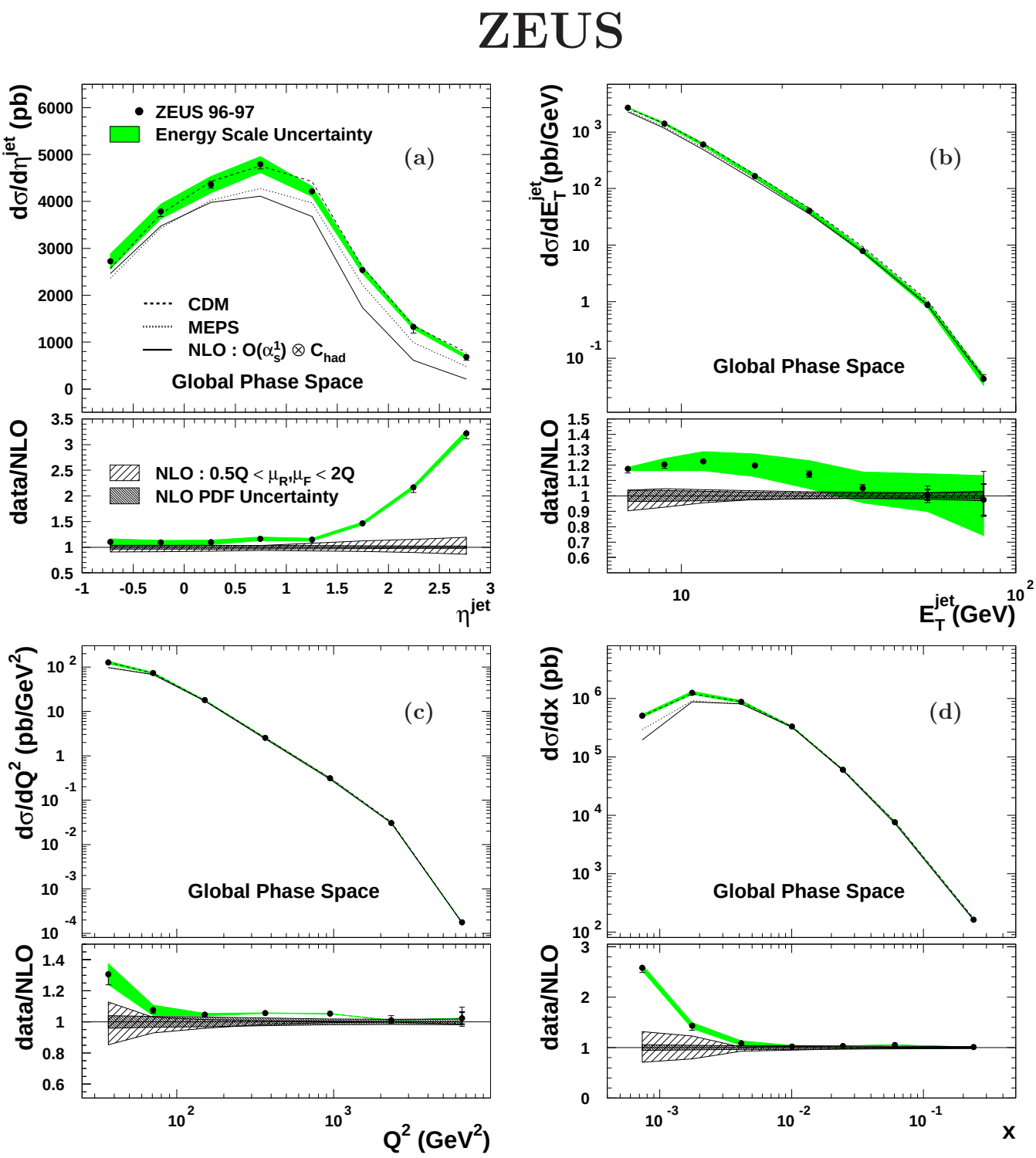

Figure 2: *Differential cross sections (dots) in the global phase space for inclusive jet production in NC DIS with $E_T^{\rm jet} > 6$ GeV, $-1 < \eta^{\rm jet} < 3$, $Q^2 > 25$ GeV^2 and $y > 0.04$ as functions of (a) $\eta^{\rm jet}$, (b) $E_T^{\rm jet}$, (c) Q^2 and (d) x. The uncertainties are generally smaller than the markers; where visible the thick error bars represent the statistical uncertainty and the thin error bars show the statistical and systematic uncertainties added in quadrature. The uncertainty in the absolute energy scale of the jets is shown separately as a shaded band. The calculations of CDM (dashed lines), MEPS (dotted lines) and $\mathcal{O}(\alpha_s)$ QCD calculations (solid lines) are shown. The lower part of each plot shows the ratio of data to the QCD calculations and the theoretical uncertainties.*

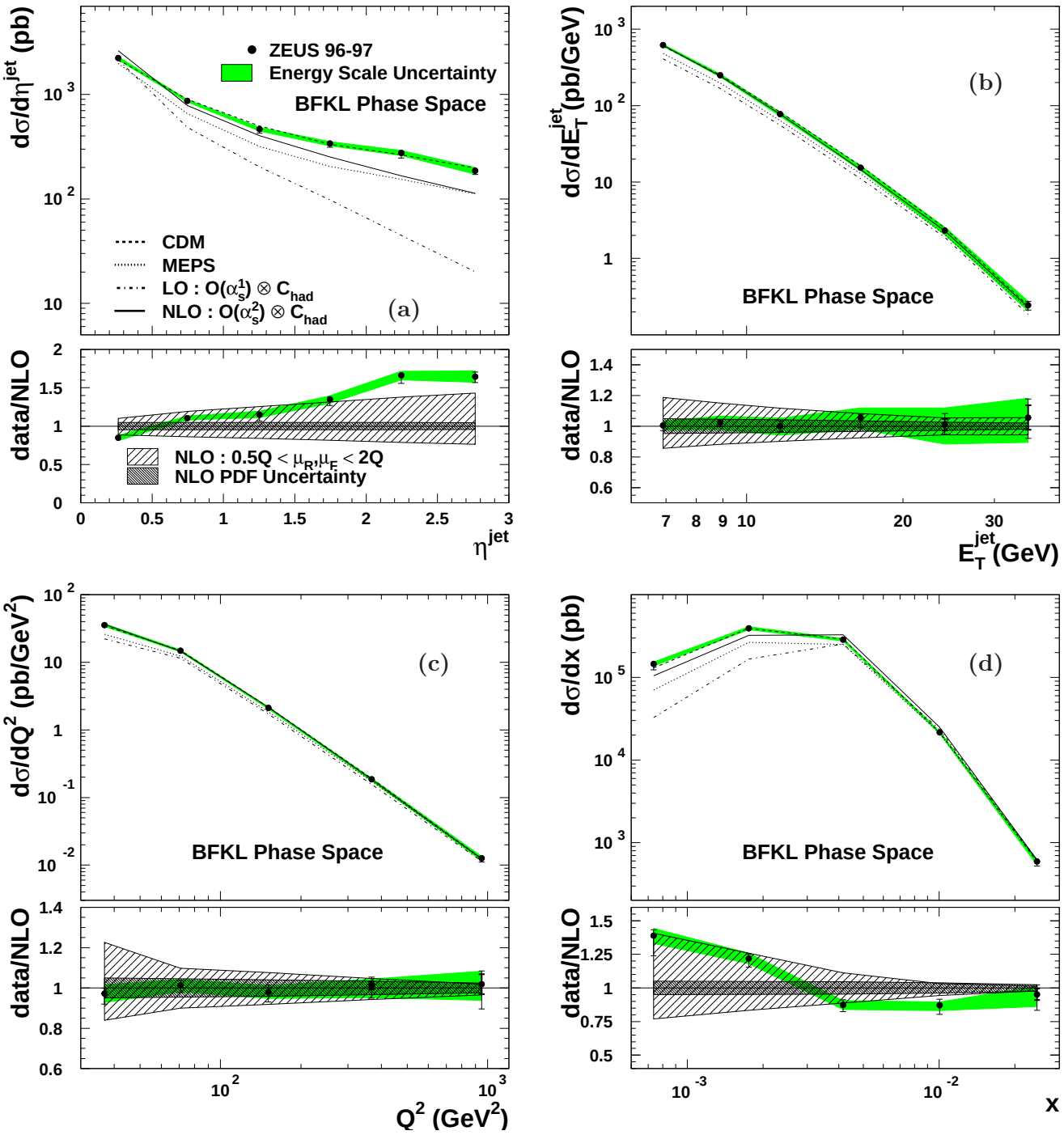

Figure 3: *Differential cross sections (dots) in the BFKL phase space for inclusive jet production in NC DIS with* $E_T^{\rm jet} > 6$ GeV, $0 < \eta^{\rm jet} < 3$, $Q^2 > 25$ GeV^2, $y > 0.04$, $\cos\gamma_h < 0$ *and* $0.5 < (E_T^{\rm jet})^2/Q^2 < 2$ *as functions of (a)* $\eta^{\rm jet}$, *(b)* $E_T^{\rm jet}$, *(c)* Q^2 *and (d)* x. *The* $\mathcal{O}(\alpha_s)$ *(dot-dashed lines) and* $\mathcal{O}(\alpha_s^2)$ *(solid lines) QCD calculations are shown. Other details are as in the caption to Fig. 2.*

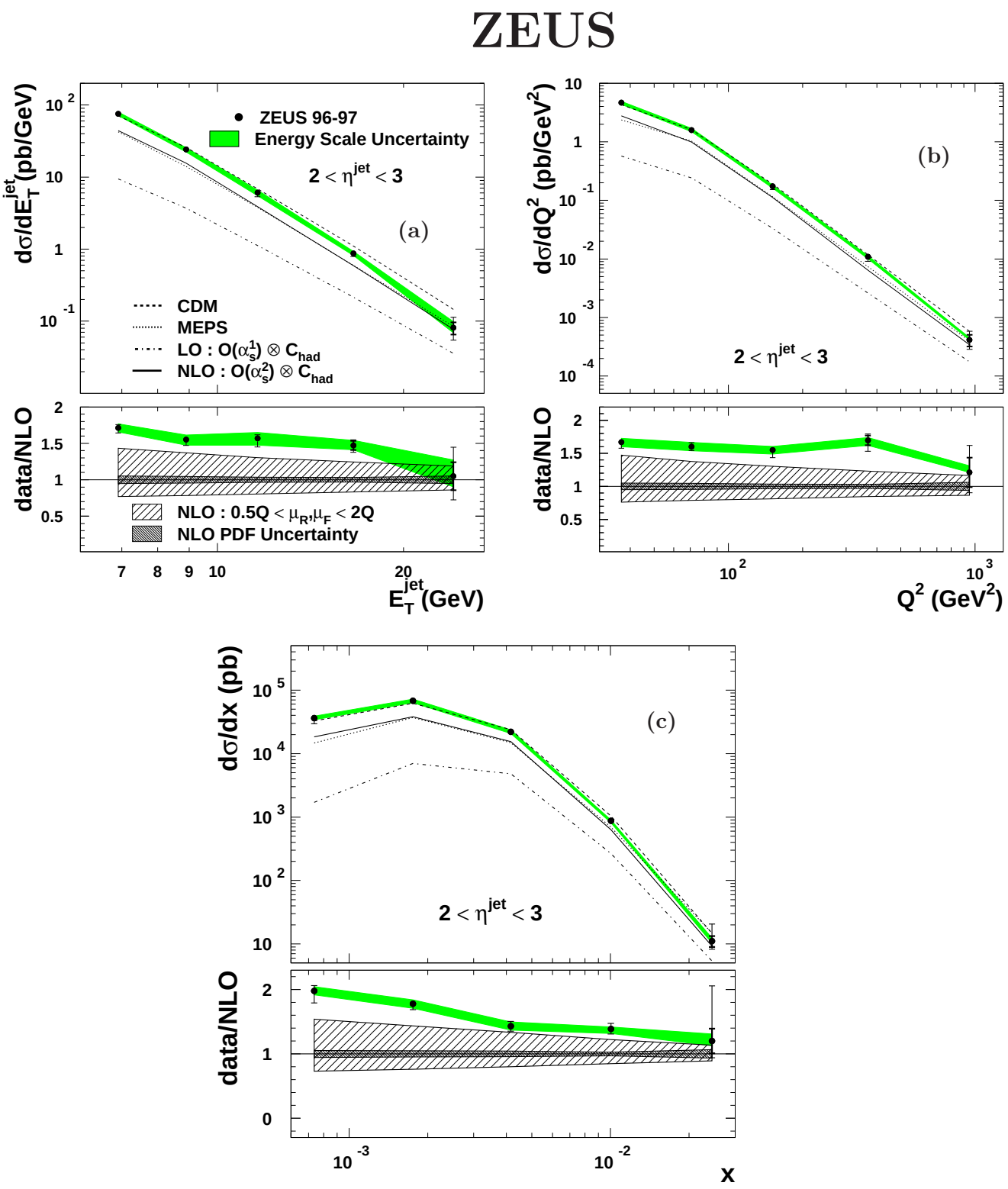

Figure 4: *Differential cross sections (dots) in the forward BFKL phase space for inclusive jet production in NC DIS with* $E_T^{\rm jet} > 6$ GeV, $2 < \eta^{\rm jet} < 3$, $Q^2 > 25$ GeV^2, $y > 0.04$, $\cos\gamma_h < 0$ *and* $0.5 < (E_T^{\rm jet})^2/Q^2 < 2$ *as functions of (a)* $E_T^{\rm jet}$, *(b)* Q^2 *and (c)* x. *The* $\mathcal{O}(\alpha_s)$ *(dot-dashed lines) and* $\mathcal{O}(\alpha_s^2)$ *(solid lines) QCD calculations are shown. Other details are as in the caption to Fig. 2.*